Available online at www.sciencedirect.com
SCIENCE DIRECT®
ELSEVIER
International Journal of Solids and Structures 41 (2004) 6853–6871
INTERNATIONAL JOURNAL OF SOLIDS and STRUCTURES
www.elsevier.com/locate/ijsolstr

High-order layerwise mechanics and finite element for the damped dynamic characteristics of sandwich composite beams

Theofanis S. Plagianakos, Dimitris A. Saravanos *

Department of Mechanical Engineering and Aeronautics, University of Patras, Patras, GR 26500, Greece

Received 13 January 2004; received in revised form 14 May 2004
Available online 3 July 2004

Abstract

A high-order discrete-layer theory and a finite element are presented for predicting the damping of laminated composite sandwich beams. The new layerwise laminate theory involves quadratic and cubic terms for approximation of the in-plane displacement in each discrete layer, while interlaminar shear stress continuity is imposed through the thickness. Integrated damping mechanics are formulated and both laminate and structural stiffness, mass and damping matrices are formed. A finite element method and a beam element are further developed for predicting the free vibration response, including modal frequencies, modal loss factors and through-thickness mode shapes. Numerical results and evaluations of the present model are shown. Modal frequencies and damping of sandwich composite beams are measured and correlated with predicted values. Finally, parametric studies illustrate the effect of core thickness and face lamination on modal damping and frequency values.

Keywords: Composite materials; Laminates; Sandwich; Beams; Damping; Modeling; Finite element; Free vibration

1. Introduction

Passive damping is a critical parameter in improving the dynamic performance of flexible structures requiring tight vibration control, fatigue endurance, aeroelastic stability and accurate positioning of devices and sensors. Polymer matrix composite materials are known to exhibit higher damping than most common metals and are preferred in lightweight structures, where passive damping may significantly improve dynamic and acoustic performance. Sandwich structures with laminated composite faces and foam cores are considered in many structural applications due to their increased flexural stiffness to mass ratio. The possibility to provide higher damping than composite structures because of the shearing of the viscoelastic core is an additional advantage. However, sandwich structures are challenging to model and analyze, due to the inhomogeneity in properties and anisotropy through the thickness, the high thickness and the shearing

* Corresponding author. Tel.: +30-2610996191; fax: +30-2610997234.
E-mail address: saravanos@mech.upatras.gr (D.A. Saravanos).

0020-7683/$ - see front matter © 2004 Elsevier Ltd. All rights reserved.
doi:10.1016/j.ijsolstr.2004.05.038

of the core. Thus, discrete-layer formulations are essential in order to sufficiently capture interlaminar shear effects on both static and damped dynamic performance.

Substantial analytical and experimental work was reported on damping mechanisms of composite laminates (e.g. Gibson and Plunkett, 1976; Ni and Adams, 1984; Saravanos and Chamis, 1990; Wren and Kinra, 1992; Alam and Asnani, 1986). Saravanos (1994) reported a linear fully layerwise damping plate theory for laminated composite plates together with semi-analytical solutions, as well as, a finite element (1993) capable of predicting the damping of thick composite plates, and the damping of composite sandwich plates with interlaminar damping layers (Saravanos and Pereira, 1992); whereas, Taylor and Nayfeh (1997) presented an analytical solution for the damped vibrational characteristics of thick composite plates. Zapfe and Lesieutre (1999) developed a linear discrete-layer beam finite element applicable to composite sandwich beams with integral damping layers. Di Sciuva and Icardi (2001) developed a high-order zig-zag analytical solution to predict the static response of sandwich beams. Meunier and Shenoi (2001) developed a single-layer higher order solution for composite sandwich plates and reported experimental results for the foam core dynamic properties, whereas Nilsson and Nilsson (2002) presented a linear discrete-layer solution and measured eigenfrequencies of sandwich beams and plates. Birman and Byrd (2002) presented two analytical methodologies for the evaluation of damping in sandwich structures. Lee and Kosmatka (2002) developed a discrete-layer triangular element for predicting damping in composite plates, including higher order terms in the displacement approximation through the thickness and presented experimental results for composite plates with an interlaminar damping layer.

The present paper describes an integrated high-order layerwise formulation and a finite element for effectively predicting the damped free-vibration response of thick composite and sandwich beams. Previous linear layerwise formulations (Saravanos, 1993, 1994) provide the basis for developing a novel expandable high-order discrete-layer formulation, in which quadratic and cubic fields are added in the kinematics of each discrete layer, while maintaining displacement compatibility. Compatibility in interlaminar stress between adjacent layers and on the free edges is further imposed, leading to a reduction of the generalized laminate displacements. Based on this framework, the generalized laminate and structural governing equations are derived, and stiffness, mass and damping matrices are formulated. An in-plane finite element method and a 2-node damped beam finite element are further formulated for the damped free-vibration analysis of sandwich beams and modal damping is predicted using the modal strain energy dissipation method. The present finite element is used to predict modal frequencies, damping and through-thickness displacement, strain and stress fields in composite and sandwich beams. Experimental modal analysis tests conducted on sandwich beams with composite faces and a foam core are presented, moreover, measured modal damping and frequencies are correlated with predicted values. Finally, the effect of face lamination and face- to-core thickness ratio on the damping of sandwich beams is studied.

2. Theoretical formulation

The following paragraphs describe the integrated multi-scale formulation, starting from the basic material equations and arriving to the prediction of the damped free-vibration response of a sandwich beam.

2.1. Governing material equations

In general the laminate layers including both composite plies and foam core are assumed to exhibit orthotropic viscoelastic behavior. Assuming harmonic loading, the off-axis complex stress component $\boldsymbol{\sigma}_c$ is provided by:

$$\boldsymbol{\sigma}_{c_i} = ([\mathbf{Q}_{c_{ij}}] + \mathrm{j}[\mathbf{Q}_{c_{im}}][\boldsymbol{\eta}_{c_{mj}}])\mathbf{S}_{c_j} \tag{1}$$

where subscripts $i, j, m = 1, \ldots, 6$ indicate stress and strain components in extended vector notation form; subscript c indicates the structural coordinate system $Oxyz$; j is the imaginary unit; $\mathbf{S}_j$, $\boldsymbol{\sigma}_i$ are the engineering strain and stress; $[\mathbf{Q}_c]$ is the off-axis storage stiffness matrix; $[\boldsymbol{\eta}_c]$ is the off-axis loss factor matrix in the structural system. The latter is related through a proper rotational transformation (Saravanos and Chamis, 1990) to the on-axis damping matrix $[\boldsymbol{\eta}_l]$ containing the four independent damping loss factors of a composite ply, describing the longitudinal damping η_{l1} (direction 11), transverse damping η_{l2} (direction 22), in-plane shear damping $\eta_{l6} = \eta_{l5}$ (directions 12 and 13) and interlaminar shear damping η_{l4} (direction 23). Reduced stiffness and damping matrices $[\mathbf{Q}^*_{ij}]$ and $[\mathbf{Q}^*_{\mathrm{d}_{ij}}]$ $(i, j = 1, 5)$ are used for the beam case, where σ_{c_1} and σ_{c_5} are the assumed non-zero stresses. The reduction method is described in Appendix A. In the remaining paragraphs, reduced matrices are used and superscript * is implied.

2.2. Kinematic assumptions

A typical laminate is assumed to be subdivided into n discrete layers as shown schematically in Fig. 1a, each discrete layer may contain either a single ply, a sublaminate, or a subply. A piecewise linear in-plane displacement field is first assumed through the laminate thickness, which maintains continuity across the discrete-layer boundaries, while allowing for different slopes in each discrete layer. Parabolic and cubic variations in the displacement field are further assumed through the thickness of each discrete layer (Fig. 1b). In this manner, the displacement field in the kth discrete layer takes the form:

$$\begin{aligned} u(x,z,t) &= U^k(x,t)\Psi_1^k(\zeta_k) + U^{k+1}(x,t)\Psi_2^k(\zeta_k) + \alpha^k(x,t)\frac{h_k}{2}(\zeta_k^2 - 1) + \lambda^k(x,t)\frac{h_k}{2}\zeta_k(\zeta_k^2 - 1) \\ w(x,z,t) &= w^{\mathrm{o}}(x,t) \end{aligned} \tag{2}$$

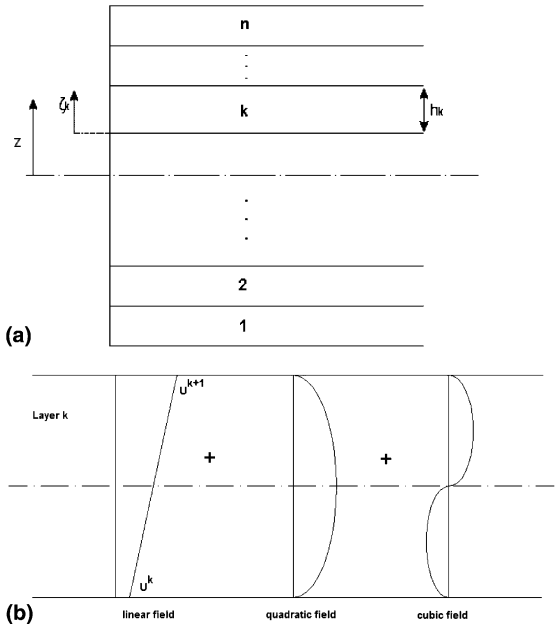

Fig. 1. Typical laminate configuration analyzed with n discrete layers. (a) Discrete layers; (b) assumed displacement field components through the thickness of a discrete layer; the linear component corresponds to a linear layerwise model.

where superscripts $k = 1, \ldots, n$ indicates the discrete layer, and o the mid-plane; The first two terms in the right hand side describe the linear displacement field; U^k, U^{k+1} are the in-plane displacements at the interfaces of each discrete layer (Saravanos and Heyliger, 1995) effectively describing the extension and rotation of the layer, and Ψ^k are linear interpolation functions through the layer thickness,

$$\begin{aligned} \Psi_1^k &= (1-\zeta_k)/2 \\ \Psi_2^k &= (1+\zeta_k)/2 \end{aligned} \tag{3}$$

The last two terms in Eq. (2) describe quadratic and cubic variations; α^k and λ^k are hyper-rotations in each discrete layer introduced by the quadratic and cubic terms, respectively, and ζ_k is the local thickness coordinate of layer k, given by:

$$\zeta_k = \frac{2}{h_k} z - \frac{z_1^k + z_2^k}{h_k} \tag{4}$$

where h_k is the discrete layer thickness, z_1 and z_2 are the z-axis coordinates of the discrete layer's bottom and top surface, respectively.

2.3. Strain–displacement relations

In the context of kinematic assumptions (2) the axial and shear strains S_1 and S_5 in each discrete layer are,

$$\begin{aligned} S_1^k &= U_{,x}^k \Psi_1^k + U_{,x}^{k+1} \Psi_2^k + \alpha_{,x}^k \frac{h_k}{2}(\zeta_k^2 - 1) + \lambda_{,x}^k \frac{h_k}{2} \zeta_k (\zeta_k^2 - 1) \\ S_5^k &= w_{,x}^{\mathrm{o}} + U^k \Psi_{1,\zeta_k}^k \frac{2}{h_k} + U^{k+1} \Psi_{2,\zeta_k}^k \frac{2}{h_k} + 2\alpha^k \zeta_k + \lambda^k (3\zeta_k^2 - 1) \end{aligned} \tag{5}$$

In the axial strain equation, $U_{,x}^k$ and $U_{,x}^{k+1}$ represent contributions of the mid-layer strain and curvature, while the last two terms the contributions of hyper-curvatures $\alpha^k{}_{,x}$ and $\lambda^k{}_{,x}$ in the discrete layer. In the interlaminar shear strain equation, the sum of the first three right hand side terms yields a constant shear term, while the last two terms provide a linear and a quadratic term through the thickness of the kth layer. The comma in the subscripts indicates differentiation.

2.4. Through-thickness compatibility

The displacement continuity at ply interfaces is self-imposed by the kinematic assumptions (2). Although, the compatibility of shear stresses on the layer interfaces and free surfaces is weakly maintained through the equations of equilibrium, shear stress compatibility conditions may be also explicitly imposed. In the latter case, transverse shear stresses should be continuous between adjacent layers, and equal to surface tractions τ_5^L, τ_5^U at the free edges,

$$\begin{aligned} &\sigma_5^k(\zeta_k = 1) = \sigma_5^{k+1}(\zeta_{k+1} = -1) \\ &\sigma_5^1(\zeta_1 = -1) = \tau_5^L \\ &\sigma_5^n(\zeta_n = 1) = \tau_5^U \end{aligned} \tag{6}$$

where n is the upper discrete layer. Imposition of these $n+1$ linear equations results in additional advantages: (1) it enables prediction of shear stresses at the ply interface; and (2) it yields a set of linear equations, thus, relating $n+1$ of the laminate DOFs to the remaining ones, the former were selected to be all λ^i, $i = 1, \ldots, n$ and the a^n. The compatibility equations, thus take the following form,

$$\begin{Bmatrix} \alpha^n \\ \lambda^i \end{Bmatrix} = [\mathbf{R}] \begin{Bmatrix} w_{,x} \\ \mathbf{U}^j \\ \boldsymbol{\alpha}^k \end{Bmatrix} \tag{7}$$

where $i = 1, \ldots, n,\ j = 1, \ldots, n+1,\ k = 1, \ldots, n-1$; $[\mathbf{R}]$ is the reduction matrix, having dimensions $(n+1) \times (2n+1)$ described in Appendix A. Inclusion of Eq. (7) into the governing laminate equations leads to the elimination of $n+1$ laminate DOFs.

2.5. Laminate matrices

The dissipated W_{dL} and stored W_{L} strain energy per unit area in the laminate during a vibration cycle are defined as follows:

$$W_{\mathrm{dL}} = \frac{1}{2} \int_{-\frac{h}{2}}^{\frac{h}{2}} \mathbf{S}_i^{\mathrm{T}} [\mathbf{Q}_{\mathrm{d}_{c_{ij}}}] \mathbf{S}_j \, \mathrm{d}z \tag{8}$$

$$W_{\mathrm{L}} = \frac{1}{2} \int_{-\frac{h}{2}}^{\frac{h}{2}} \mathbf{S}_i^{\mathrm{T}} [\mathbf{Q}_{c_{ij}}] \mathbf{S}_j \, \mathrm{d}z \tag{9}$$

where $i, j = 1, 5$ and $[\mathbf{Q}_{\mathrm{d}_c}] = [\mathbf{Q}_c][\boldsymbol{\eta}_c]$. Combining Eqs. (2)–(9) and collecting the coefficients in the common degrees of freedom between adjacent layers (see Appendix A) we arrive to the final forms of dissipated and stored strain energy in the laminate:

$$W_{\mathrm{dL}} = \frac{1}{2} \{\mathbf{S}_{\mathrm{Lr}_1}\} [\mathbf{G}_{\mathrm{dr}}] \{\mathbf{S}_{\mathrm{Lr}_1}\} + \frac{1}{2} \{\mathbf{S}_{\mathrm{Lr}_5}\} [\mathbf{F}_{\mathrm{dr}}] \{\mathbf{S}_{\mathrm{Lr}_5}\} \tag{10}$$

$$W_{\mathrm{L}} = \frac{1}{2} \{\mathbf{S}_{\mathrm{Lr}_1}\} [\mathbf{G}_r] \{\mathbf{S}_{\mathrm{Lr}_1}\} + \frac{1}{2} \{\mathbf{S}_{\mathrm{Lr}_5}\} [\mathbf{F}_r] \{\mathbf{S}_{\mathrm{Lr}_5}\} \tag{11}$$

where $[\mathbf{G}_r]$, $[\mathbf{F}_r]$, and $[\mathbf{G}_{\mathrm{dr}}]$, $[\mathbf{F}_{\mathrm{dr}}]$ are $(2n+1) \times (2n+1)$ generalized stiffness and damping laminate matrices containing in-plane and interlaminar stiffness and damping terms, respectively; subscript r indicates the stiffness and damping matrix reduction performed by imposing the stress compatibility equation (7); and $\{\mathbf{S}_{\mathrm{Lr}_1}\} = \{w_{,xx}, U^1{}_{,x}, \ldots, U^{n+1}{}_{,x}, \alpha^1{}_{,x}, \ldots, \alpha^{n-1}{}_{,x}\}$ and $\{\mathbf{S}_{\mathrm{Lr}_5}\} = \{w_{,x}, U^1, \ldots, U^{n+1}, \alpha^1, \ldots, \alpha^{n-1}\}$ are the reduced laminate strain vectors. The kinetic energy of the laminate takes the form:

$$K_{\mathrm{L}} = \frac{1}{2} \{\dot{\mathbf{u}}_{\mathrm{Lr}}\}^{\mathrm{T}} [\mathbf{m}_{\mathrm{Lr}}] \{\dot{\mathbf{u}}_{\mathrm{Lr}}\} \tag{12}$$

where $[\mathbf{m}_{\mathrm{Lr}}]$ is the reduced laminate inertia matrix and $\{\mathbf{u}_{\mathrm{Lr}}\} = \{w, U^1, \ldots, U^{n+1}, \alpha^1, \ldots, \alpha^{n-1}\}$ is the reduced laminate displacement vector, as described in Appendix A.

It is noted, that for the simple case of a single discrete layer, the present theory effectively reduces to the well known single-layer higher order theory with cubic terms in the in-plane displacement approximation (Reddy, 1997) with compatibility equation (6) containing only the last two surface traction conditions. The corresponding damping matrices for the single-layer case are described in Appendix A.

2.6. Equations of motion

The equations of motion of the undamped system are defined in variational form, using the Hamilton's principle, as:

$$\int_{t_1}^{t_2}\left(-\int_V \delta\mathbf{S}_i^{\mathrm{T}}\boldsymbol{\sigma}_i\,\mathrm{d}V+\int_V\delta\left(\frac{1}{2}\rho\dot{u}_j^2\right)\mathrm{d}V+\int_{\Gamma_\sigma}\delta\bar{\boldsymbol{u}}_j\bar{\boldsymbol{\tau}}_j\,\mathrm{d}\Gamma\right)\mathrm{d}t=0 \tag{13}$$

where $i=1,5$ and $j=1,3$. After substituting constitutive equations (1), (2) and (5) into the previous equation, integration through the thickness yields the equations of motion in terms of generalized strains and laminate matrices:

$$\int_{t_1}^{t_2}\left(-\int_0^{L_x}\delta W_{\mathrm{L}}\,\mathrm{d}x-\int_0^{L_x}\delta W_{\mathrm{dL}}\,\mathrm{d}x+\int_0^{L_x}\delta K_{\mathrm{L}}\,\mathrm{d}x+\int_0^{L_x}\delta\bar{\boldsymbol{u}}\bar{\boldsymbol{\tau}}\,\mathrm{d}x\right)\mathrm{d}t=0 \tag{14}$$

where δW_{L} is the variation of laminate strain energy in Eq. (11), δW_{dL} is the variation of the laminate dissipated energy, and δK_{L} is the variation of laminate kinetic energy. The conservative and dissipated strain energy terms result from the first term of Eq. (13), and the latter strongly depend on the assumed viscoelastic constitutive law. For the case of harmonic vibration with a composite constitutive equation (1), the dissipated and stored strain energy take finally the forms provided by Eqs. (10) and (11), respectively.

2.7. Finite element formulation

Based on the previous equations of motion (14), a finite element based solution was developed. C_1 continuous shape functions $H(x)$ were implemented in the local approximation of the transverse displacement w^{o}, while C_0 shape functions $N(x)$ were used for the remaining DOFs. The compatibility equations (6) or (7) imply that in order to maintain continuity in the eliminated hyper-rotations λ^i $(i=1,\ldots,n)$ and a^n, the slope of the transverse displacement $w^{\mathrm{o}}_{,x}$ should also remain continuous along element boundaries, hence the requirement for C_1 continuity on w^{o}. The use of C_1 shape functions also results in continuity in the constant shear strain component of Eq. (5). In this manner, the local approximations of the generalized state variables in the element take the following type:

$$\begin{aligned}
U^k(x,t)&=\sum_{i=1}^{L}U^{ki}(t)N^i(x)\\
\alpha^m(x,t)&=\sum_{i=1}^{L}\alpha^{mi}(t)N^i(x)\\
w^{\mathrm{o}}(x,t)&=\sum_{i=1}^{L}\left(w^{\mathrm{o}i}(t)H_1^i(x)+\frac{L_{\mathrm{e}}}{2}w^{\mathrm{o}i}_{,x}(t)H_2^i(x)\right)
\end{aligned} \tag{15}$$

where $k=1,\ldots,n+1$and $m=1,\ldots,n-1$; L_{e} denotes the element length. A 2-node ($L=2$) beam element was further developed and encoded employing linear interpolation functions N^i and cubic Hermitian polynomials H_1^i, H_2^i.

2.8. Beam damping

Substituting Eqs. (10)–(12) and (15) into the governing equations of motion (14), and assuming harmonic motion, we arrive to the final form of the discrete system describing the free-vibration response of the beam:

$$-\omega^2[\mathbf{M}]\{\boldsymbol{V}\}+j[\mathbf{C}]\{\boldsymbol{V}\}+[\mathbf{K}]\{\boldsymbol{V}\}=0 \tag{16}$$

where $\{\boldsymbol{V}\}$ are the amplitude vectors; $[\mathbf{M}]$, $[\mathbf{C}]$ and $[\mathbf{K}]$ are the inertia, damping and stiffness matrices of the beam, respectively, obtained from Eq. (14) after substituting Eqs. (10)–(12) and (15) and collecting the common terms. The resultant expression for the element damping matrix, is described in Appendix A. In

the case of frequency independent damping, Eq. (16) can be solved directly, to yield the complex eigenvalues of the system, from which modal frequencies and damping can be extracted. Moreover, in the case of relatively low damping, the modal strain energy dissipation approach can be used, which assumes that the undamped mode shapes do not differ substantially from those of the damped system. The modal loss factor associated with the mth order mode η_m is the ratio of dissipated to stored strain modal energy of the mth mode:

$$\eta_m = \frac{\int_0^{L_x} \Delta W_{\mathrm{L}m}\,\mathrm{d}x}{\int_0^{L_x} W_{\mathrm{L}m}\,\mathrm{d}x} \tag{17}$$

The numerical solution of Eq. (16) for $[\mathbf{C} = 0]$ provides the undamped natural frequencies and the modal displacement vectors of the beam. The modal loss factor of the beam is then calculated from the ratio of the respective dissipated and maximum stored energies:

$$\eta_m = \frac{\boldsymbol{V}_m^{\mathrm{T}}[\mathbf{C}]\boldsymbol{V}_m}{\boldsymbol{V}_m^{\mathrm{T}}[\mathbf{K}]\boldsymbol{V}_m} \tag{18}$$

Eqs. (16)–(18) are consistent with the assumed constitutive material behavior described by Eq. (1). Besides its previous stated limitations, the modal strain energy approach provides simple damping measures of the structure, and for this reason it was adopted in this work. Other formulations implementing time-domain damping models (e.g. Bagley and Torvik, 1986; Zapfe and Lesieutre, 1999) can be alternatively considered, which do not suffer from the previous limitations and may capture frequency dependence, however, such approaches exceed the scope of present work and are left as a topic of future research.

3. Experiments

Sandwich beams were fabricated with a foam (f) core (DIAB Klegecell R grade foam) and Glass/Polyester (Gl/Pl) composite faces of [0/f/0] and [90/f/90] laminations, and their modal characteristics were subsequently measured. The beam specimens were cut from a [0/f/0] plate, which was fabricated by hand lay-up and their dimensions were $L_x = 860$ mm, $b = 50$ mm, $h = 35$ mm, with b denoting specimen's width. The thicknesses of each of the faces and the core were $h_{\mathrm{f}} = 2.5$ mm and $h_{\mathrm{c}} = 30$ mm, respectively. The elastic and damping properties of the Gl/Pl composite (Chrisochoidis, 2001) and foam were also measured. The dimensions of the tested foam specimen were $L_x = 1140$ mm, $b = 50$ mm, $h = 20$ mm.

3.1. Experimental procedure

The experimental setup is shown schematically in Fig. 2. The specimens were suspended by wires to reproduce near free–free boundary conditions in order to eliminate friction damping in the supports. The excitation was applied using either a medium electromagnetic shaker or an impact hammer, both having a load cell attached. The beams were excited at position 1 (mid-length) or 2 (free-end) and a miniature (1g) accelerometer was used to measure the acceleration at positions 1 or 2 in order to acquire both symmetric and antisymmetric modes. In the case of the shaker, a swept sine force was applied to excite the specimen. The signals of the load cell and the accelerometer were first amplified, then digitized through a high speed data acquisition board and finally processed using FFT software to obtain the power spectra and frequency response function (FRF) of the beam. The measured FRFs were further correlated with a known parametric model of complex exponential terms, each term approximating an individual mode with known modal parameters (frequency and damping), such that the least squares error between the model and measured FRFs was minimized. Through this correlation, the modal frequencies and damping coefficients

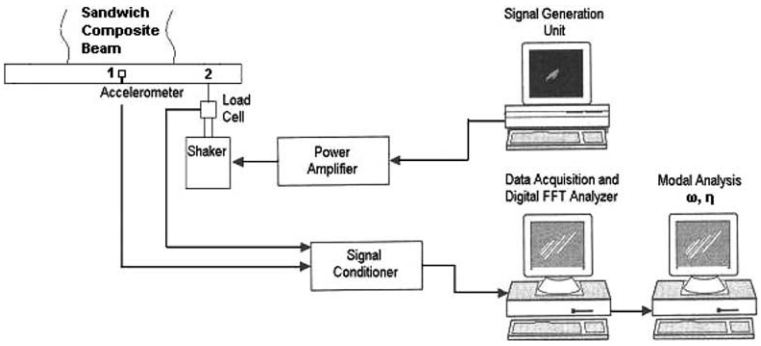

Fig. 2. Experimental configuration for measuring modal frequencies and damping of the sandwich beams.

of the tested specimens were extracted. A similar procedure was used to extract the elastic and damping coefficients of the Gl/Pl composite and of the foam, shown in Table 1.

4. Results and discussion

This section presents static and modal analysis results obtained using the developed finite element and comparisons with predictions of other single-layer and layerwise theories. The latter include a linear discrete-layer theory and finite element which has been extensively correlated with exact plate solutions (Saravanos and Heyliger, 1999). Modal damping and frequencies are predicted for thick composite beams, composite beams with ISD110 interlaminar damping layers and composite sandwich beams with foam core. The mechanical properties of all materials are shown in Table 1.

4.1. Static response of sandwich beam

The static response of a simply-supported sandwich beam analyzed by Di Sciuva and Icardi (2001) using a layerwise analytical solution was modeled. The applied transverse sinusoidal pressure had the form:

$$p(x) = p_0 \sin\left(\frac{\pi x}{L}\right)$$

The beam had a thickness aspect ratio $L/h = 4$ and a core to face thickness ratio $h_c/h_f = 4$. It was modeled using 11 finite elements, and 12 discrete layers through the thickness, each representing an individual ply or the core. Fig. 3a and b illustrate the predicted distribution of in-plane axial stress σ_1 and interlaminar shear stress σ_5 through the thickness of the beam in normalized form, respectively. Predicted stress is normalized as

$$\bar{\sigma}_{xz} = \frac{\sigma_{xz}(0,z)}{p_0}; \quad \bar{\sigma}_{xx} = \frac{\sigma_{xx}(L/2,z)}{p_0}$$

Very good correlation is observed between the present layerwise element and the analytical solution (Di Sciuva and Icardi, 2001) for both axial and interlaminar shear stress, indicating that the current element can accurately predict stress in thick sandwich beam structures, where stress distribution through the thickness can be complicated.

Table 1
Elastic and damping properties of materials considered

	Gl/Pl composite	3 M 110 polymer	Klegecell R foam
Elastic properties			
E_{11} (GPa)	25.8	113.0e−3	35.0e−3
E_{22} (GPa)	8.7	113.0e−3	35.0e−3
E_{33} (GPa)	8.7	113.0e−3	35.0e−3
G_{23} (GPa)	2.4	38.0e−3	12.3e−3
G_{13} (GPa)	3.5	38.0e−3	12.3e−3
G_{12} (GPa)	3.5	38.0e−3	12.3e−3
ν_{12}	0.34	0.49	0.40
ν_{13}	0.34	0.49	0.40
ν_{23}	0.47	0.49	0.40
Damping properties			
η_{l1} (%)	0.65	1.60	2.40
η_{l2} (%)	2.34	1.60	2.40
η_{l4} (%)	2.89	16.00	3.00
η_{l6} (%)	2.89	16.00	3.00
Mass density ρ (kg/m^3)	1672	1000	45

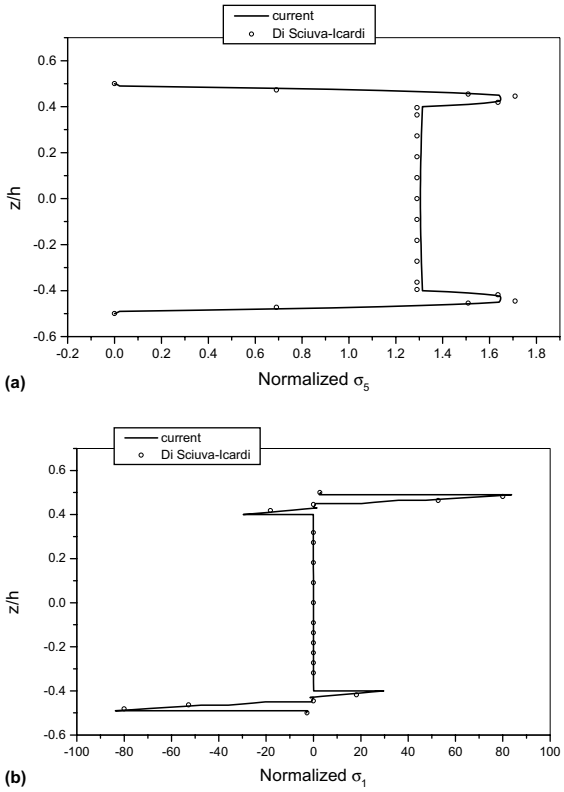

Fig. 3. Predicted static response of a simply-supported sandwich beam under sinusoidal loading. (a) interlaminar shear stress; (b) axial stress through the thickness.

4.2. [0/90/0] Beam

The static response of a [0/90/0] Glass/Polyester (Gl/Pl) moderately thick ($L/h = 10$) composite beam subject to 3-point bending was predicted. The beam was 150 mm long and was modeled using six elements and three discrete layers through the thickness. Each layer represented a laminate ply and had a thickness of 5 mm. Each node had 8 structural degrees of freedom, namely the transverse deflection and its slope, four axial displacements, one for each hidden node through thickness, and the α^1, α^2 from the discrete layers 1 and 2, respectively. A transverse line load of 39.37 N/mm was considered at the center of the beam. The predicted transverse deflection and the interlaminar shear strain and stress fields through the thickness at 1/4 of the length are presented in Fig. 4a–c and compared with finite element results of a linear discrete-layer theory (Saravanos and Heyliger, 1995), which uses $n = 15$ discrete layers and subsequently 16 structural degrees of freedom per node. Excellent correlation between the two models is observed, which shows that the present high-order discrete-layer damping theory can accurately capture interlaminar shear effects and calculate strains and stresses at the ply interfaces. As expected, there is continuity in predicted stress between adjacent layers (Fig. 4c) while both shear strain and stress vanish at the stress-free edges. The contribution of linear and high-order terms on the calculation of total interlaminar strain is also illustrated

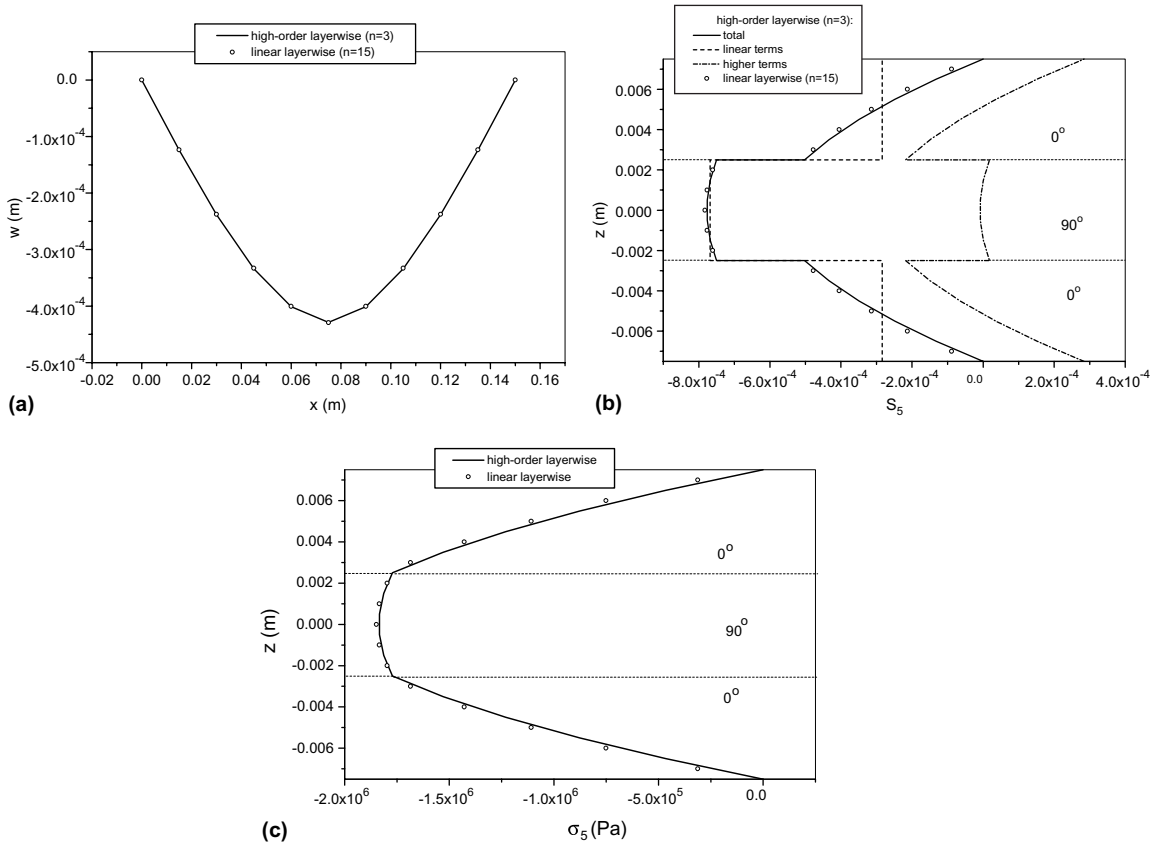

Fig. 4. Predicted static response of simply-supported [0/90/0] Gl/Pl beam under 3-point bending. (a) Transverse deflection; (b) distribution of interlaminar shear strain through the thickness, including linear and high-order terms; (c) distribution of interlaminar shear stress through the thickness.

in Fig. 4b. The excellent results obtained and the minimal number of laminate degrees of freedom used by the present laminate model vs. the linear discrete-layer theory, indicate the improved computational efficiency of the former vs. the latter.

Natural frequencies and modal loss factors of the beam in unsupported conditions were predicted and compared with results of a single-layer first-order shear damping shell theory (FSDT) (Plagianakos and Saravanos, 2003), which has been previously validated with exact plate solutions (Saravanos and Heyliger, 1999). A 10×1 shell finite element model was used. Fig. 5a and b demonstrate the effect of thickness aspect ratio on the normalized natural frequency ($\omega_{\text{norm}} = \omega bL/h$) and modal loss factor of the first two bending modes, respectively. Very good correlation is observed for thin sections (high thickness aspect ratios), whereas, for thick beams the higher order discrete-layer theory seems to provide higher predictions of damping and lower predictions of modal frequencies than the first-order shear theory, apparently, due to the improved representation of interlaminar shear effects.

4.3. $[\theta_2/-\theta_2/i/\theta_2/-\theta_2]_s$ clamped-free beam

The effect of ply angle on modal damping of a $[\theta_2/-\theta_2/\text{i}/\theta_2/-\theta_2]$ Glass/Polyester moderately thick ($L/h = 50$) clamped-free beam was studied; i indicates interlaminar damping layer (3 M 110 viscoelastic damping polymer) with mechanical properties shown in Table 1. The beam had a length of 225 mm and was modeled using five discrete layers through the thickness, one layer for each of the three restraining sublaminates and one layer for each of the two damping layers. The thickness of each damping layer was

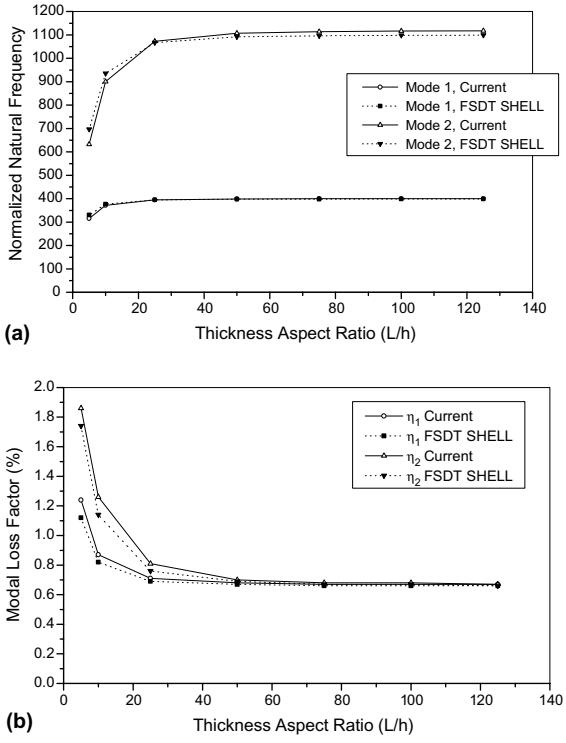

Fig. 5. Effect of thickness aspect ratio on the damped response of a free [0/90/0] Gl/Pl beam. (a) Normalized bending frequencies; (b) bending modal loss factors.

0.25 mm. The enhancement of modal damping by adding viscoelastic layers for the three first bending modes of the beam with respect to the ply angle is shown in Fig. 6. For the higher bending modes, where interlaminar shear effects are more dominant, modal damping almost quintuplicates in the $\theta = 0$ laminations due to increased shear in the viscoelastic layers imposed by stiffer restraining composite faces. Furthermore, as the mode number increases a more uniform variation of damping with respect to the fiber orientation angle is observed, providing great advantage and flexibility towards the design of laminated composite beams with interply damping layers exhibiting high stiffness and damping.

4.4. Free–free sandwich beams

Modal frequencies and damping of the tested [0/f/0] and [90/f/90] beams were predicted and correlated with measured values. The longitudinal modal loss factor η_{l1} of the foam was also measured and found to be frequency independent for frequencies over 100 Hz (Fig. 7). The shear modal loss factor of the foam was measured from a single torsional mode, near 150 Hz. Thus, the foam damping values shown in Table 1, correspond to the measured constant damping values over 100 Hz. The sandwich beams were modeled using 20 elements in the axial direction and five discrete layers through the thickness, arranged as follows:

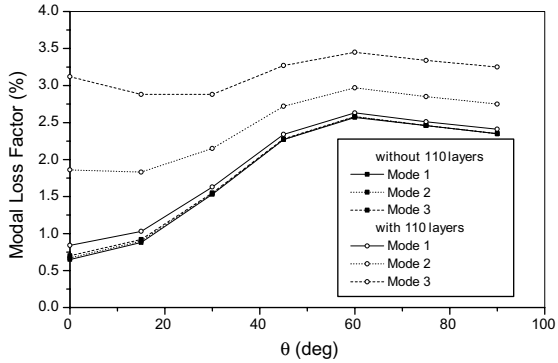

Fig. 6. Effect of ply angle on modal damping of the first three bending modes of a cantilever $[\theta_2/-\theta_2/\mathrm{i}/\theta_2/-\theta_2]_s$ Gl/Pl beam with interply damping layers.

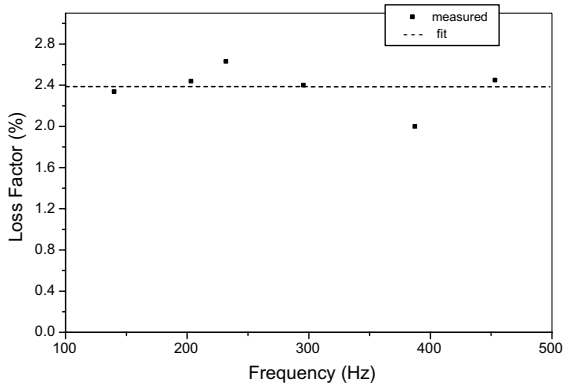

Fig. 7. Measured axial (or flexural) damping of the foam core.

one 2.3 mm thick layer for each face, one 30 mm thick layer for the core and two 0.23 mm thick layers for the region between face and core, being reach in matrix due to fabrication. In Fig. 8a and b predicted modal damping values for the eight first bending modes of the beams are presented. Measured damping values obtained using shaker and hammer excitation are also shown. Very good correlation is observed in the [0/f/0] case; whereas, in the [90/f/90] case some deviation exists, especially near low frequencies, possibly due to imperfections in the fabrication of the Gl/Pl composite faces and some frequency effects. However, in both cases the present method has captured the modal damping trend to increase at higher modes, as interlaminar shear effects become more dominant, reaching eventually a saturation plateau. This point will be further discussed in the following case.

4.5. Clamped-free sandwich beam

The through-thickness modal response of a similar to the previous case [0/f/0] sandwich beam with Gl/Pl composite faces and foam core was studied. The beam was 500 mm long, had a thickness aspect ratio L/h of 14.3 and was modeled using 20 elements and $n = 3$ discrete layers through the thickness. The core to face thickness aspect ratio h_{co}/h_{fo} was 6.25. Fig. 9a and b show predicted distributions of modal displacement and interlaminar strain, respectively, through the thickness near the clamped end for the three first bending

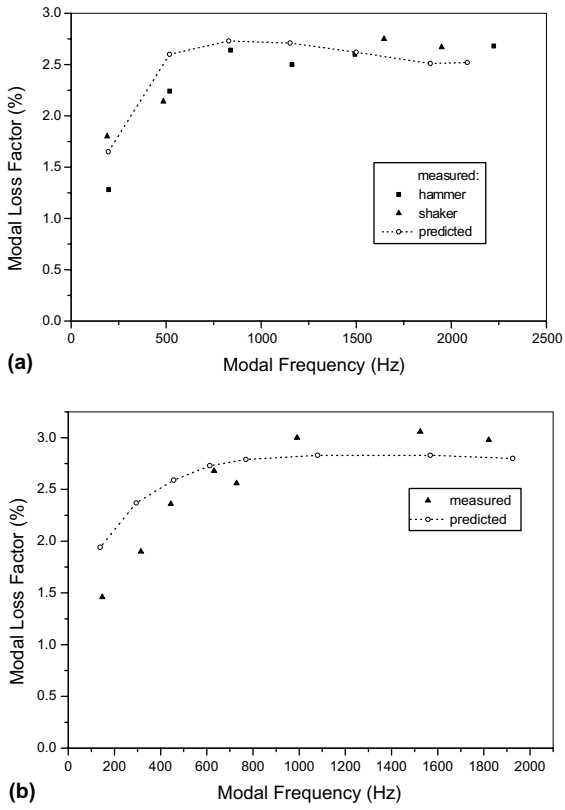

Fig. 8. Predicted and measured modal damping and frequencies for the eight first bending modes of free Gl/Pl sandwich composite beams, (a) [0/f/0] and (b) [90/f/90].

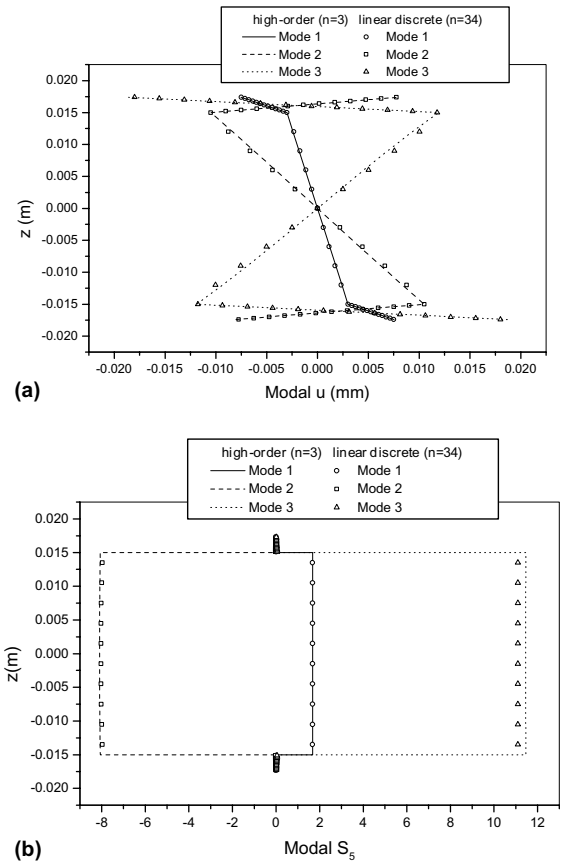

Fig. 9. Predicted modal distribution through the thickness of a cantilever [0/f/0] Gl/Pl sandwich composite beam. (a) Modal displacement; (b) modal interlaminar shear strain, near the clamped end.

modes. Results were compared to those obtained using a linear layerwise beam FE with $n = 34$ discrete layers (Saravanos and Heyliger, 1995) with very good agreement. The effect of core to face thickness aspect ratio on damping of the three first bending modes is presented in Fig. 10a. There is a baseline composite damping, upon which damping is added as the core gets thicker due to shear effects, which is clearly shown in Fig. 10b, where the fundamental modal interlaminar shear stress distribution through the thickness near the clamped end is presented. Higher modes exhibit higher damping due to the presence of increased interlaminar shear. There is also a thickness ratio threshold for each individual mode, beyond which damping seems to be rather insensible to core thickness. This saturation may probably indicate that interlaminar shear effects become less dominant than interlaminar normal effects (σ_3 action), which the present theory does not capture.

In closing, the presented numerical predictions and their comparison with various analytical, numerical and experimental results has successfully quantified the accuracy range of the present method. The robust analytical capabilities of the present laminate theory were illustrated through the analysis of various laminations, thick composite beams, thick sandwich beams with foam cores and composite beams with compliant damping layers. In all previous cases, the present approach seemingly provided very good displacement and stress predictions through the laminate, using a minimal number of discrete layers and degrees of freedom.

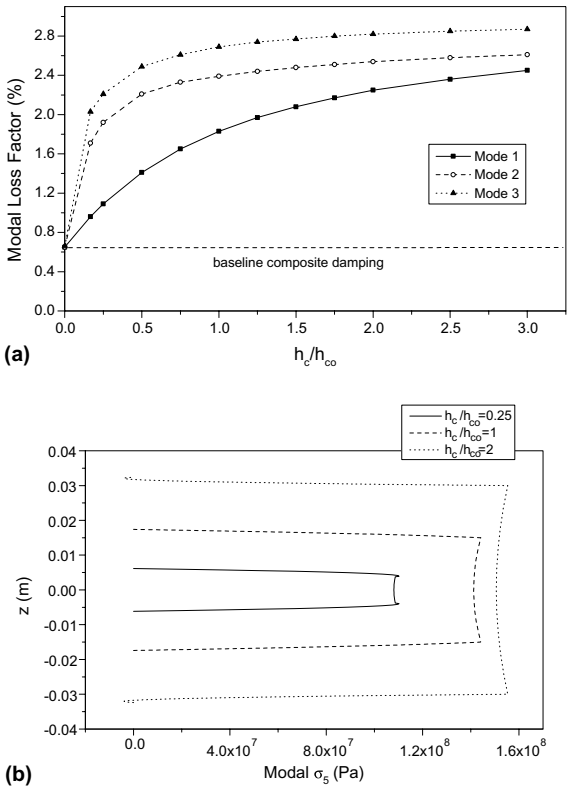

Fig. 10. Effect of core thickness on the damped modal response of a cantilever [0/f/0] Gl/Pl sandwich composite beam. (a) Damping of the three first bending modes; (b) interlaminar shear stress distribution of the fundamental mode near the clamped end.

5. Summary

Unified mechanics and a finite element for predicting modal damping and natural frequencies of thick composite and sandwich beams were presented. A discrete-layer higher order theory satisfying compatibility in interlaminar shear stress was developed and modal damping was calculated by the modal strain energy dissipation method. Various validations illustrated the accuracy of the developed formulation.

The strong effect of ply orientation on the modal damping of a composite beam with interply viscoelastic damping layers was investigated and higher bending modes were found to exhibit increased damping compared to the fundamental, which also varied more uniformly with ply angle. The improved damping behavior of foam sandwich beams was quantified both analytically and experimentally. The strong effect of core to face thickness aspect ratio on the modal damping of a sandwich beam was also studied, and it was observed that as the core thickness increases, the modal damping first will also increase until a saturation plateau is reached. Overall, the results have demonstrated the damping potential of composite sandwich beam structures, as well as, the capability of developed layerwise damping theory to accurately analyze their global and local damped dynamic response.

Acknowledgements

Part of this work was supported by ENK6-CT2000-00320 ENERGIE program. The authors gratefully acknowledge this support, as well as, the support of Mr. Theodore Kossivas of Geoviologiki SA, who provided the sandwich specimens. The authors want also to thank Research Assistant Nikos Chrysochoidis, for his valuable help with the experimental work.

Appendix A

A.1. Equivalent ply properties

Stiffness. The equivalent reduced ply stiffness matrix $[\mathbf{Q}_c^*]$ is calculated from the full compliance matrix $[\mathbf{s}_c]$ by maintaining the elements corresponding to the non-zero stress components (σ_1, σ_5) as follows:

$$[\mathbf{Q}_c^*] = [\mathbf{s}_c^*]^{-1} = \begin{bmatrix} s_{c_{11}} & 0 \\ 0 & s_{c_{55}} \end{bmatrix}^{-1} = \begin{bmatrix} \mathbf{Q}_{c_{11}}^* & 0 \\ 0 & \mathbf{Q}_{c_{55}}^* \end{bmatrix} \tag{A.1}$$

Damping. The dissipated energy per unit volume per cycle within a ply is given by the following form:

$$W_c = \frac{1}{2}\mathbf{S}_c^{\mathrm{T}}[\boldsymbol{\eta}_c][\mathbf{Q}_c]\mathbf{S}_c = \frac{1}{2}\boldsymbol{\sigma}_c^{\mathrm{T}}[\mathbf{s}_c][\boldsymbol{\eta}_c]\boldsymbol{\sigma}_c \tag{A.2}$$

where $[\boldsymbol{\eta}_c]$ is the off-axis ply damping matrix. By maintaining only the elements of $[\mathbf{s}_c][\boldsymbol{\eta}_c]$ corresponding to σ_1, σ_5 non-zero stress components, the equivalent off-axis ply damping matrix is obtained as follows:

$$[\boldsymbol{\eta}_c^*] = [\mathbf{Q}_c^*]([\mathbf{s}_c][\boldsymbol{\eta}_c]) = \begin{bmatrix} \boldsymbol{\eta}_{c_{11}}^* & 0 \\ 0 & \boldsymbol{\eta}_{c_{55}}^* \end{bmatrix} \tag{A.3}$$

The equivalent loss-stiffness matrix is:

$$[\mathbf{Q}_{\mathrm{d}_c}^*] = [\mathbf{Q}_c^*][\boldsymbol{\eta}_c^*] \tag{A.4}$$

A.2. Discrete-layer matrices, ith layer

In-plane stiffness matrix, dimension (4×4)

$$\left\{\mathbf{S}_{l_1}^i\right\}^{\mathrm{T}}[\mathbf{G}_l^i]\left\{\mathbf{S}_{l_1}^i\right\} = \sum_{m=1}^{n_{\mathrm{p}}^i} \int_{\zeta_m^i}^{\zeta_{m+1}^i} \{\mathbf{S}_1^i\}^{\mathrm{T}} Q_{11}^m \{\mathbf{S}_1^i\} \frac{h_i}{2}\, \mathrm{d}\zeta^i \tag{A.5}$$

Interlaminar shear stiffness matrix (5×5)

$$\left\{\mathbf{S}_{l_5}^i\right\}^{\mathrm{T}}[\mathbf{F}_l^i]\left\{\mathbf{S}_{l_5}^i\right\} = \sum_{m=1}^{n_{\mathrm{p}}^i} \int_{\zeta_m^i}^{\zeta_{m+1}^i} \{\mathbf{S}_5^i\}^{\mathrm{T}} Q_{55}^m \{\mathbf{S}_5^i\} \frac{h_i}{2}\, \mathrm{d}\zeta^i \tag{A.6}$$

In-plane damping matrix (4×4)

$$\left\{\mathbf{S}_{l_1}^i\right\}^{\mathrm{T}}[\mathbf{G}_{\mathrm{d}_l}^i]\left\{\mathbf{S}_{l_1}^i\right\} = \sum_{m=1}^{n_{\mathrm{p}}^i} \int_{\zeta_m^i}^{\zeta_{m+1}^i} \{\mathbf{S}_1^i\}^{\mathrm{T}} Q_{11}^m \eta_{11}^m \{\mathbf{S}_1^i\} \frac{h_i}{2}\, \mathrm{d}\zeta^i \tag{A.7}$$

Interlaminar shear damping matrix (5 × 5)

$$\left\{\mathbf{S}_{l_5}^i\right\}^{\mathrm{T}}[\mathbf{F}_{\mathrm{d}_1}^i]\left\{\mathbf{S}_{l_5}^i\right\} = \sum_{m=1}^{n_{\mathrm{p}}^i}\int_{\zeta_m^i}^{\zeta_{m+1}^i}\left\{\mathbf{S}_5^i\right\}^{\mathrm{T}} Q_{55}^m \eta_{55}^m \left\{\mathbf{S}_5^i\right\}\frac{h_i}{2}\,\mathrm{d}\zeta^i \tag{A.8}$$

Generalized density matrix (5 × 5)

$$\left\{\dot{\mathbf{u}}_l^i\right\}^{\mathrm{T}}[\mathbf{m}_l^i]\left\{\dot{\mathbf{u}}_l^i\right\} = \sum_{m=1}^{n_{\mathrm{p}}^i}\int_{\zeta_m^i}^{\zeta_{m+1}^i}\left\{\dot{\mathbf{u}}^i\right\}^{\mathrm{T}}\rho_m^i\left\{\dot{\mathbf{u}}^i\right\}\frac{h_i}{2}\,\mathrm{d}\zeta^i \tag{A.9}$$

where n_{p}^i is the total number of plies in the ith layer and $m = 1,\ldots,n_{\mathrm{p}}^i$; $\{\mathbf{S}_{l_1}^i\} = \{U_{,x}^i, U_{,x}^{i+1}, \alpha_{,x}^i, \lambda_{,x}^i\}$ and $\{\mathbf{S}_{l_5}^i\} = \{w_{,x}, U^i, U^{i+1}, \alpha^i, \lambda^i\}$ are the generalized strain vectors of the ith layer, whereas $\{\mathbf{S}_1^i\}$, $\{\mathbf{S}_5^i\}$ are the strains in the ith layer described in Eq. (5); $\{\mathbf{u}_l^i\} = \{w^{\mathrm{o}}, U^i, U^{i+1}, \alpha^i, \lambda^i\}$ is the generalized displacement vector of the ith layer, whereas $\{\mathbf{u}^i\}$ is the displacement vector of the ith layer described in Eq. (2), including both w and u.

A.3. Laminate matrices encompassing all previous submatrices through-the-thickness

In-plane stiffness, damping matrices $[\mathbf{G}]$, $[\mathbf{G}_{\mathrm{d}}]$, dimensions $(3n+1)\times(3n+1)$; interlaminar shear stiffness, damping matrices $[\mathbf{F}]$, $[\mathbf{F}_{\mathrm{d}}]$, dimensions $(3n+2)\times(3n+2)$ where n is the total number of layers of the laminate, built as follows:

$$\{\mathbf{S}_{\mathrm{L}_1}\}^{\mathrm{T}}[\mathbf{G}]\{\mathbf{S}_{\mathrm{L}_1}\} = \sum_{i=1}^{n}\{\mathbf{S}_{l_1}^i\}^{\mathrm{T}}[\mathbf{G}_l^i]\{\mathbf{S}_{l_1}^i\} \tag{A.10}$$

$$\{\mathbf{S}_{\mathrm{L}_5}\}^{\mathrm{T}}[\mathbf{F}]\{\mathbf{S}_{\mathrm{L}_5}\} = \sum_{i=1}^{n}\{\mathbf{S}_{l_5}^i\}^{\mathrm{T}}[\mathbf{F}_{\mathrm{l}}^i]\{\mathbf{S}_{l_5}^i\} \tag{A.11}$$

$$\{\mathbf{S}_{\mathrm{L}_1}\}^{\mathrm{T}}[\mathbf{G}_{\mathrm{d}}]\{\mathbf{S}_{\mathrm{L}_1}\} = \sum_{i=1}^{n}\{\mathbf{S}_{l_1}^i\}^{\mathrm{T}}[\mathbf{G}_{\mathrm{d}_1}^i]\{\mathbf{S}_{l_1}^i\} \tag{A.12}$$

$$\{\mathbf{S}_{\mathrm{L}_5}\}^{\mathrm{T}}[\mathbf{F}_{\mathrm{d}}]\{\mathbf{S}_{\mathrm{L}_5}\} = \sum_{i=1}^{n}\{\mathbf{S}_{l_5}^i\}^{\mathrm{T}}[\mathbf{F}_{\mathrm{d}_1}^i]\{\mathbf{S}_{l_5}^i\} \tag{A.13}$$

$\{\mathbf{S}_{\mathrm{L}_1}\} = \{U_{,x}^1,\ldots,U_{,x}^{n+1},\alpha_{,x}^1,\ldots,\alpha_{,x}^n,\lambda_{,x}^1,\ldots,\lambda_{,x}^n\}$ and $\{\mathbf{S}_{\mathrm{L}_5}\} = \{w_{,x}, U^1,\ldots,U^{n+1},\alpha^1,\ldots,\alpha^n,\lambda^1,\ldots,\lambda^n\}$ are the generalized laminate strain vectors.

A.4. Compatibility system (built from Eq. (6))

$$[\boldsymbol{P}]\begin{Bmatrix} w_{,x} \\ U^j \\ \boldsymbol{\alpha}^i \\ \boldsymbol{\lambda}^i \end{Bmatrix} = 0 \tag{A.14}$$

where $i = 1, \ldots, n$, $j = 1, \ldots, n+1$; $\boldsymbol{P}$ is the compatibility matrix, having dimensions $(n+1) \times (2n+1)$. Eq. (A.14), upon partitioning and rearrangement of the $[\boldsymbol{P}]$ matrix, provides Eq. (7).

A.5. Beam element damping matrix

Combining Eq. (15) with Eq. (10) and taking into account the reduced generalized laminate in-plane and interlaminar strains, the beam element damping matrix is derived,

$$[C_{\mathrm{e}}^{ij}] = \int_{L_{\mathrm{e}}} \left([b^i]^{\mathrm{T}} [G_{\mathrm{dr}}] [b^j] + [b_{\mathrm{s}}^i]^{\mathrm{T}} [F_{\mathrm{dr}}] [b_{\mathrm{s}}^j] \right) \mathrm{d}x \tag{A.15}$$

where i, j indicate the nodes of the finite element and $[b]$ and $[b_{\mathrm{s}}]$ are the shape function matrices corresponding, respectively, to the reduced in-plane and interlaminar shear strains. The element stiffness and mass matrices are obtained in a similar manner. The element matrices are then used to synthesize the structural stiffness, damping and mass matrices, $[\mathbf{K}]$, $[\mathbf{C}]$ and $[\mathbf{M}]$, respectively, of Eq. (16).

A.6. Single-layer case

In the case of a single-layer through thickness, the theoretical framework developed reduces to the high-order shear deformation theory (Reddy, 1997) in the case of a beam. The in-plane displacement through-thickness approximation in Eq. (2) becomes,

$$u(x,z,t) = U^1(x,t)\Psi_1(\zeta) + U^2(x,t)\Psi_2(\zeta) + \alpha(x,t)\frac{h}{2}(\zeta^2 - 1) + \lambda(x,t)\frac{h}{2}\zeta(\zeta^2 - 1) \tag{A.16}$$

with $\alpha = 0$ and $\lambda = \frac{1}{3}\left(-w_{,x} + \frac{U^1 - U^2}{h} \right)$, as mandated from the two last compatibility equation (6) assuming traction-free outer surfaces. In the context of Eq. (10) the reduced laminate in-plane and interlaminar shear damping matrices $[G_{\mathrm{dr}}]$ and $[F_{\mathrm{dr}}]$, respectively, are 3×3 matrices and $\{\mathbf{S}_{\mathrm{Lr}_1}\} = \{w_{,xx}, U^1{}_{,x}, U^2{}_{,x}\}$ and $\{\mathbf{S}_{\mathrm{Lr}_5}\} = \{w_{,x}, U^1, U^2\}$ are the reduced laminate strain vectors.

References

Alam, N., Asnani, N.T., 1986. Vibration and damping analysis of fibre reinforced composite material plates. Journal of Composite Materials 20 (1), 2–18.

Bagley, R.L., Torvik, P.J., 1986. On the fractional calculus model of viscoelastic behavior. Journal of Rheology 30 (1), 133–155.

Birman, V., Byrd, L.W., 2002. Analytical evaluation of damping in composite and sandwich structures. AIAA Journal 40 (8), 1638–1643.

Chrisochoidis, N., 2001. Measurement of Damping Coefficients of Glass/Polyester Composites. MS Thesis, Department of Mechanical Engineering and Aeronautics, University of Patras, Greece.

Di Sciuva, M., Icardi, U., 2001. Numerical assessment of the core deformability effect on the behavior of sandwich beams. Composite Structures 52 (1), 41–53.

Gibson, R.F., Plunkett, R., 1976. Dynamic mechanical behaviour of fiber reinforced composites: measurements and analysis. Journal of Composite Materials 10, 325–341.

Lee, D.G., Kosmatka, J.B., 2002. Damping analysis of composite plates with zig-zag triangular element. AIAA Journal 40 (6), 1211–1219.

Meunier, M., Shenoi, R.A., 2001. Dynamic analysis of composite sandwich plates with damping modelled using high-order shear deformation theory. Composite Structures 53 (4), 243–254.

Ni, R.G., Adams, R.D., 1984. The damping and dynamic moduli of symmetric laminated composite beams—theoretical and experimental results. Journal of Composite Materials 18 (2), 104–121.

Nilsson, E., Nilsson, A.C., 2002. Prediction and measurement of some dynamic properties of sandwich structures with honeycomb and foam cores. Journal of Sound and Vibration 251 (3), 409–430.

Plagianakos, T.S., Saravanos, D.A., 2003. Mechanics and finite elements for the damped dynamic characteristics of curvilinear laminates and composite shell structures. Journal of Sound and Vibration 263 (2), 399–414.

Reddy, J.N., 1997. Mechanics of Laminated Composite Plates—Theory and Analysis. CRC Press Inc., New York.

Saravanos, D.A., 1993. Analysis of passive damping in thick composite structures. AIAA Journal 31 (8), 1503–1510.

Saravanos, D.A., 1994. Integrated damping mechanics for thick composite laminates and plates. Journal of Applied Mechanics 61 (2), 375–383.

Saravanos, D.A., Chamis, C.C., 1990. Mechanics of damping for fiber composite laminates including hygro-thermal effects. AIAA Journal 28 (10), 1813–1819.

Saravanos, D.A., Heyliger, P.R., 1995. Coupled layerwise analysis of composite beams with embedded piezoelectric sensors and actuators. Journal of Intelligent Material Systems and Structures 6 (3), 350–363.

Saravanos, D.A., Heyliger, P.R., 1999. Mechanics and computational models for laminated piezoelectric beams, plates and shells. Applied Mechanics Reviews 52 (10), 305–320.

Saravanos, D.A., Pereira, J.M., 1992. Effects of interply damping layers on the dynamic characteristics of composite plates. AIAA Journal 30 (12), 2906–2913.

Taylor, T.W., Nayfeh, A.H., 1997. Damping characteristics of laminated thick plates. Journal of Applied Mechanics 64 (1), 132–138.

Wren, C.G., Kinra, V.K., 1992. Axial damping in metal–matrix composites I: a theoretical model and its experimental verification. Experimental Mechanics 32 (2), 172–178.

Zapfe, J.A., Lesieutre, G.A., 1999. A discrete layer beam finite element for the dynamic analysis of composite sandwich beams with integral damping layers. Computers and Structures 70 (2), 647–666.